Remote Sensing of Environment 199 (2017) 39–50

Contents lists available at ScienceDirect

Remote Sensing of Environment

journal homepage: www.elsevier.com/locate/rse

Propensity for erosion and deposition in a deltaic wetland complex: Implications for river management and coastal restoration

Reda Amer [a], Alexander S. Kolker [b,a,*], Annelise Muscietta [a]

[a] Department of Earth and Environmental Science, Tulane University, New Orleans, LA 70115, United States
[b] Louisiana Universities Marine Consortium, 8124 Highway 56, Chauvin, LA 70344, United States

ARTICLE INFO

Article history:
Received 20 October 2016
Received in revised form 21 May 2017
Accepted 27 June 2017
Available online 14 July 2017

ABSTRACT

The Mississippi River Delta is one of the most rapidly changing area on Earth, with large areas experiencing land loss and smaller areas experiencing loss. While some of the drivers of these changes are well known (high rates of relative sea level rise, reduced sediment inputs, canal dredging), debate exists about other drivers. One area that has received substantial attention is the role of, "river diversions," areas where sediments and water are diverted from the Mississippi River into degrading wetlands with the hope of reinitiating deltaic land building processes. Some authors have argued that diversions lead to reduced shear strengths of wetland soils that make them more vulnerable to storm driven erosion, while other authors have argued that sediments from river diversions will develop stable land. This study examined this controversy in the Cubits Gap Subdelta, an analogue for a large (>1420 m^3 s^{-1}) river diversion by testing the hypothesis that areas of land gain, and/or resilience to erosion occurred in areas that actively received river sediments and as a result had mineral rich soils with high shear strength. To accomplish this, a Normalized Difference Water Index (NDWI) was developed for Landsat-7 Enhanced Thematic Mapper (ETM+) and Landsat-8 Operational Land Imager (OLI) images. The NDWI was calculated from (Blue − SWIR) / (Blue + SWIR), where SWIR is the shorter wavelength, and yielded land/water boundary maps with 30 m resolution. Results indicate that land gain occurred predominantly in the riverside section of this subdelta where sediments were imported from Mississippi River crevasses and/or dredging. Land loss typically occurred in the distal regions of the subdelta, which had lower levels of sediment supply and greater wave exposure. Sediment geotechnical analyses revealed land loss pixels generally correlated sediments with to high organic contents ($9.0 \pm 1.9\%$), water contents ($54.8 \pm 3.7\%$) and salinity (6.5 ± 2.0 PSU), with low shear strengths (5.7 ± 0.8 kN m^{-2}) and low bulk density (0.6 ± 0.8 g cm^{-3}), whereas land gain pixels generally correlate with low organic content ($3.9 \pm 0.6\%$), water content ($38.1 \pm 4.2\%$) high shear strength (10.9 ± 4.1 kN m^{-2}) and bulk density (1.00 ± 0.1 g cm^{-3}). This study suggests plans to restore the region by partially diverting the flow of the Mississippi River will be most successful if they carry high loads of sediment, and that concerns about the integrity of fresh marsh may be unwarranted if those marshes are sediment rich.

1. Introduction

The modern deltaic plain of Louisiana consists of approximately 25,000 km^2 of wetlands, bays, rivers, and bayous that were created as the Mississippi River deposited sediments in the shallows reaches of the northern Gulf of Mexico over the past 7000 years (Roberts, 1997). During the past century, nearly 4877 km^2, or ~25% of the land area of coastal Louisiana, converted from land to open water (Couvillion et al., 2011). This land loss makes the Mississippi River Delta one of the most rapidly changing environments on earth (Giosan et al., 2014; Syvitski and Saito, 2007). The causes of this land loss are complex and often interact. Reduced sediment inputs, coupled with high rates of subsidence have resulted in a situation in which many marshes can no longer accrete at rates necessary to keep pace with sea-level rise, which leads to land loss (Reed, 2002, LACPRA 2017, Day et al., 2007, Kolker et al., 2011). Hurricanes, wave driven erosion, canal construction, saltwater intrusion, eutrophication and invasive species have also played a major role in driving land loss in Louisiana (Howes et al., 2010; Turner, 1997; Darby and Turner, 2008). The processes that drive land loss, and land gain, in the Mississippi River Delta are potentially significant globally given that deltas across the planet are shrinking and sinking as a result of human activities (Syvitski and Saito, 2007; Giosan et al., 2014).

To offset this ongoing land loss, the State of Louisiana crafted a "Comprehensive Master Plan for a Sustainable Coast" (LACPRA, 2017).

* Corresponding author at: Department of Earth and Environmental Science, Tulane University, New Orleans, LA 70115, United States.
E-mail addresses: ramer1@tulane.edu (R. Amer), akolker@lumcon.edu (A.S. Kolker), amusciet@tulane.edu (A. Muscietta).

http://dx.doi.org/10.1016/j.rse.2017.06.030

This plan pursues multiple strategies for restoring wetlands and protecting existing wetlands and coastal communities. One noteworthy strategy is to partially divert the flow of the Mississippi river, which should reinitiate the natural land building processes that originally formed the delta (LACPRA 2017, Roberts, 1997, Kim et al., 2009). This strategy of, "river diversions," is based, in part, on observations that the few areas of delta growth are the areas that actively receive river water including the outlets of the Atchafalaya River, regions of the Birdsfoot Delta of the Mississippi River, and small areas around the Caernarvon and Davis Pond Freshwater Diversions (Wellner et al., 2005; Wells and Coleman, 1987; Roberts, 1997). A summary of these diversion structures is presented in Table 1.

There has been marked controversy surrounding river diversions and their role in coastal change. Some authors have suggested that freshwater diversions adversely affect marsh stability because they results in fresh, eutrophic marshes with plant roots with reduced structural integrity relative to salt marshes (Teal et al., 2012; Howes et al., 2010; Kearney et al., 2011). These authors often point to the Caernarvon Diversion and the response of marshes in nearby Breton Sound to Hurricane Katrina. Here, diversion-influenced freshwater marshes were readily eroded by the storm, whereas nearby uninfluenced salt marshes were more resilient to the storms impacts (Barras, 2006; Howes et al., 2010). This was attributed to the increased root structure, and corresponding increase in shear strength of salt marsh vegetation relative to fresh marsh vegetation. Some authors have cited these observations when suggesting that river diversions are not a worthwhile tool to restore the Mississippi River Delta (Turner et al., 2007; Kearney et al., 2011).

However, other authors have pointed out that the Caernarvon Diversion does not transport large quantities of sediment to wetlands, given its relatively small discharge (Table 1), and shallow invert depth (Day et al., 2016a). This opposing view holds that it is the dearth of mineral sediments rather than the inputs of nutrient rich freshwater that is primarily responsible for the weakened marshes. Those ascribing to this viewpoint suggest that larger and deeper diversions, which transport greater quantities of both sediment and water, should result in greater land development, and marshes that are more resistant to erosion (Day et al., 2016b; Tornqvist et al., 2007).

Remote sensing technology has been used to identify changes in land and water area in the Mississippi River Delta, on time scales that range from multi-decadal to annual (e.g. Britsch and Dunbar, 1993; Barras et al., 2003; Couvillion et al., 2011), to event/seasonal scale (Barras, 2006). This has been accomplished using moderate resolution systems such as Landsat TM to high resolution systems such as QuickBird; IKONOS, and GeoEYE-1 (Palaseanu-Lovejoy et al., 2011 and Palaneasu-Lovejoy et al., 2013). Most of these earlier studies employed principal components (PCA), independent components analysis (ICA), and an analysis of tasseled cap transformation (TCT) components to developed expanded set of water and vegetation. This work used Landsat-based indices such as blue ratio, Braud index, green normalized difference water index (GNDWI = (Green − NIR) / (Green + NIR)), normalized difference vegetation index (NDVI = (NIR − Red) / (NIR + Red)), normalized difference water index (NDWI = (NIR − SWIR) / (NIR + SWIR)), simple and inverse ratio, and near infrared (Blue/NIR) ratio to produce continuous fractional water maps that are classified into land/water categories using an optimization procedure (Barras et al., 2003; Atkinson and Mahony, 2004; Palaseanu-Lovejoy et al., 2011). Finally, classified images from different time periods were subtracted from each other to determine the amount and percentage area change.

Table 1
Active and planned sediment diversions in Louisiana, including their original purpose and mean annual water discharge (Allison and Meselhe, 2010; Allison et al., 2012; LACPRA, 2017).

Diversion name	Purpose	Water (km^3/year)
Atchafalaya River Delta		
Wax Lake Outlet	Flood control	109
Main Atchafalaya River	Flood control	129
Mississippi River Delta		
West Bay	Land building	33
Cubit's Gap	Natural	52
Baptiste Collette	Natural	49
Bonnet Carre Spillway	Flood control	2
Davis Pond	Salinity control	3
Caernarvon	Salinity control	2
Bohemia Spillway	Flood control	1
Planned		
Mid Barataria	Land building	~67
Mid Breton	Land building	~31
Ama	Land building	~45

Land loss studies have used the spectral water index, which is a numerical indicator derived from two or more visible and shortwave-infrared (SWIR) spectral bands of the electromagnetic spectrum to determine the boundaries between land and water bodies. The NDWI is derived from the SWI and has values that range from −1 to 1, where positive values indicate that the cover type is water and negative if the cover type is non-water. An appropriate threshold of the index has to be established to separate water bodies from other land-cover features based on the spectral characteristics (Ji et al., 2009). McFeeters (1996) adopted the format of the normalized difference vegetation index (NDVI), and developed the normalized difference water index (NDWI), defined as:

$$NDWI = (B_{Green} - B_{NIR})/(B_{Green} + B_{NIR}) \tag{1}$$

Where zero was set as the threshold, the cover type is water if NDWI > 0 and it is non-water if NDWI ≤ 0.

Rogers and Kearney (2004) used red and SWIR bands to produce NDWI, given by:

$$NDWI = (B_{red} - B_{SWIR})/(B_{red} + B_{SWIR}) \tag{2}$$

Xu (2006) modified McFeeters' NDWI, in which the SWIR band was used to replace the NIR band, the threshold value for MNDWI was set to zero, given by:

$$MNDWI = (B_{Green} - B_{SWIR})/(B_{Green} + B_{SWIR}) \tag{3}$$

Ouma and Tateishi (2006) tested five different forms of NDWIs using the reflectance bands of Landsat TM/ETM for detecting and mapping the changes of lake shorelines. They ranked the NDWIs in order of the worst to the best performance for detecting water features as follow:

$$NDWI\text{-}1 = (B_7 - B_5)/(B_7 + B_5) \tag{4}$$

$$NDWI\text{-}2 = (B_4 - B_2)/(B_4 + B_2) \tag{5}$$

$$NDWI\text{-}3 = (B_5 - B_4)/(B_5 + B_4) \tag{6}$$

$$NDWI\text{-}4 = (B_5 - B_2)/(B_5 + B_2) \tag{7}$$

$$NDWI\text{-}5 = (B_7 - B_2)/(B_7 + B_2) \tag{8}$$

Ji et al. (2009) tested all of the above mentioned NDWIs to know which NDWI indices give best result for delineating water features, and to determine the appropriate NDWI threshold so that the water, non-water, and mixture features can be distinguished. Their results indicated that the NDWI calculated from ($B_{Green} - B_{SWIR}$) / ($B_{Green} + B_{SWIR}$), where SWIR is the shorter wavelength region (1.2 to 1.8 μm), which is equivalent to Landsat spectral bands ($B_2 - B_5$) / ($B_2 + B_5$) has the most stable threshold. The present study develops a new algorithm for determining the fraction land and water that builds on these earlier studies, but which yields results with greater precision.

One intriguing place to investigate the processes that drive land loss and land gain in the Mississippi River Delta is the Cubit's Gap Subdelta wetland complex, which functions in an analogous manner to the diversions envisioned by Louisiana's Master Plan (Table 1; LACPRA, 2017; Kim et al., 2009, Wells and Coleman, 1987). This ~200 km^2 fan-shaped wetland complex is connected hydrologically connected to the Mississippi River through a 1.2 km wide crevasse channel. This channel, Cubit's Gap, has an average discharge of ~1650 $m^3\ s^{-1}$ (58,000 $ft^3\ s^{-1}$), and many of the large diversions envisioned by Louisiana's Master Plan are carry between 1400 and 2100 $m^3\ s^{-1}$ (50,000 $ft^3\ s^{-1}$–75,000 $ft^3\ s^{-1}$; LACPRA, 2017). The vegetation within Cubit's Gap Subdelta ranges is dominantly fresh and intermediate marsh, with fresher marshes located towards the proximal end of the delta and intermediate marsh located towards the distal end (Fig. 1). The CGSD developed downstream of an artificial crevasse located 5.3 km above Head of Passes that was created in 1862, and which was originally ~120 m wide (Wells and Coleman, 1987). Over the ensuing century, the crevasse expanded and the system built 193 km^2 of land by 1946, after which the area experienced ~100 km^2 of net land loss (Wells and Coleman, 1987). Despite this land loss, there were some areas of land gain, including areas downstream of 24 artificial crevasses that were put in place between 1983 and 1995, and which led to the development of 2.7 km^2 of land during that time (Boyer and Turner, 1995).

In order to address the controversy surrounding river diversions and their potential role as creators of land (e.g. Kim et al., 2009, LACPRA 2017) or drivers of wetland loss (e.g. Kearney et al., 2011), this study developed novel methods for examining land area changed and coupled these observations with in situ geotechnical measurements. The previously published Normalized Difference Water Index (NDWI) (Xu, 2006) could not identify the mixed land/water pixels from pure land and pure water pixels. This study developed a modified Landsat NDWI for mapping sub-pixel land/water boundaries for accurately calculating land loss and land gain in the coastal areas. These methods were used evaluate the hydrodynamic and geotechnical parameters that are associated with land loss or gain in river influenced and non-river influenced settings. More specifically, this study tested the hypothesis that areas of land gain, and/or resilience to erosion occurred in areas that actively received river sediments and as a result had mineral rich soils with high shear strength. Alternatively, degrading marshes in regions experiencing land loss, were hypothesized to occur in marshes with less river influence, higher organic contents, and reduced shear strength.

2. Methods

2.1. Data

Land loss and land gain was determined for the period 2000–2015, during which 11 tropical cyclones passed within 150 km of the study region, of which 6 were hurricanes. (Not included in this count is Hurricane Ike, which passed outside of the study region, but which nonetheless produced a storm surge in coastal Louisiana that was similar in magnitude to that of Hurricane Gustav; Hurricane Ivan was counted once, even though it passed through the Gulf of Mexico twice.) In contrast the period 1984–1999 experienced only 7 tropical storms, of which 5 were hurricanes. In this study, this team of authors used the visible/near-infrared (VNIR) and shortwave infrared (SWIR) bands of Landsat-7 Enhanced Thematic Mapper (ETM^+) for an image collected on October 28, 2000; and a Landsat-8 Operational Land Imager (OLI) image was collected on October 14, 2015. The two images were selected to have similar environmental conditions; they were acquired on the same time of year (October), and have similar spectral and spatial resolution, and similar water levels (Supplementary Table 1). SPOT-7 high resolution image acquired on October 13, 2015 at 16:6:37 (only one day before the Landsat OLI image) for the study area was used for validating the results of calculated NDWI. The multispectral image of SPOT

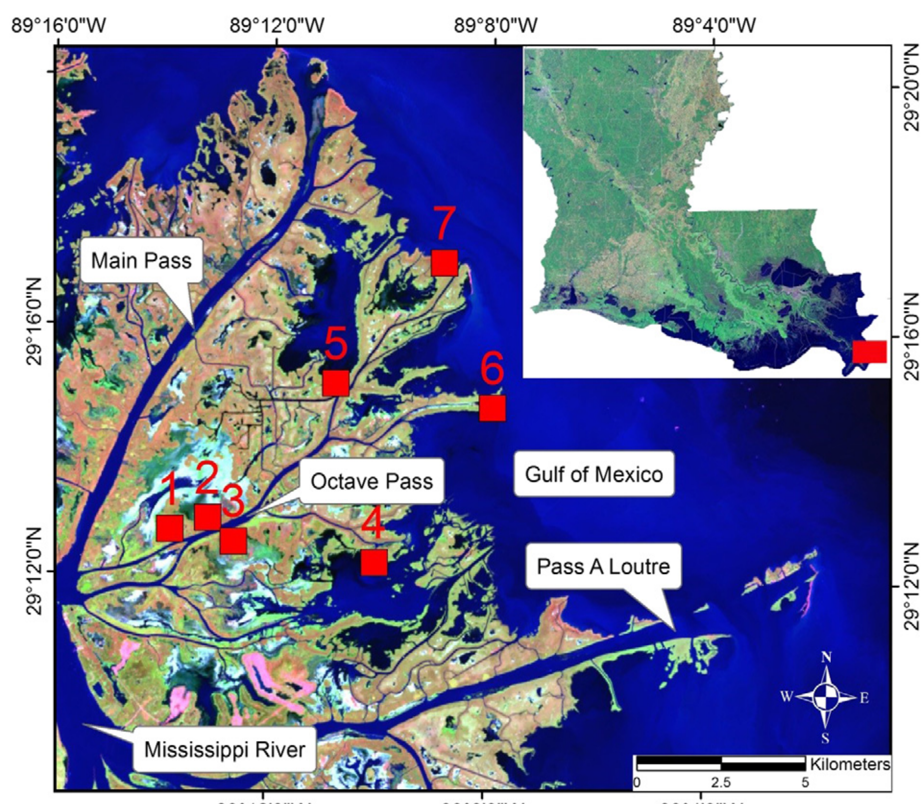

Fig. 1. Location of Cubit's Gap Subdelta and surrounding water bodies on Landsat OLI image bands 7, 5, 3 in RGB. Red squares are locations of field sites. Louisiana image is from USGS.

consists of 4 bands in blue, green, red, and near-infrared wavelengths at 6 m pixel size.

2.2. Normalized Difference Water Index (NDWI)

The Landsat ETM$^+$ and OLI images were radiometrically calibrated to the top-of-atmosphere reflectance (scaled 0.0 to 1.0) using the image's gains, offsets, solar irradiance, sun elevation, and acquisition time defined in the metadata, and we also compared the Landsat TOA reflectance images with the surface reflectance images. The design of a spectral water index was based on the fact that deep water absorbs most of the SWIR and reflects a small portion of the visible light; shallow water reflects more visible light and less SWIR; vegetation and soil on the other hand absorb most of the visible light, and reflects a large portion of the SWIR. Given that the highest reflectance of water is in the blue-wavelength and the lowest reflectance is in the SWIR (Supplementary Figs. 1, 2 and 3), one can propose a general formula of the NDWI as the normalized difference between the blue band and the SWIR band

$$\mathrm{NDWI} = (B_{\mathrm{Blue}} - B_{\mathrm{SWIR}})/(B_{\mathrm{Blue}} + B_{\mathrm{SWIR}}) \tag{9}$$

Where SWIR is the shorter wavelength region (1.55–1.75 μm); equivalent bands in Landsat-7 ETM$^+$ NDWI = (B1 − B5) / (B1 + B5); and equivalent bands in Landsat-8 OLI WI = (B2 − B6) / (B2 + B6).

2.3. Image classifications

In order to derive a land/water map at the 30-m scale, the resulting fractional NDWI maps were classified into land/water categories using an ISODATA unsupervised classifier (Mather, 2004; Memarsadeghi et al., 2006). ISODATA calculates class means evenly distributed in the data space, and then iteratively clusters the remaining pixels using minimum distance techniques. Landsat ETM$^+$ and OLI NDWI were classified into three classes, water, non-water, and mixed-water. A confusion (error) matrix was used to show the accuracy of classification results of Landsat ETM$^+$ and OLI by comparing a classification result with the ground truthed regions of interest. A confusion matrix is an effective way to represent accuracy in that the accuracies of each category are plainly described along with both the errors of inclusion (commission errors) and errors of exclusion (omission errors) present in the classification (Congalton, 1991). Overall accuracy, producer's accuracy, user's accuracy and Kappa statistics are generally reported (Foody, 2002; Plourde and Congalton, 2003). Water, non-water, and mixed-water classes were considered for accuracy assessment with the minimum of 1000 sample point for each category. Overall accuracy, user's and producer's accuracies, and the Kappa statistics were derived from the error matrices to find the reliability and accuracy of the maps produced.

2.4. Change detection analysis

Quantification of the percent land change from 2000 to 2015 was done by image subtraction method by subtracting classes from the other (Jensen, 1996; Coppin et al., 2004; Klemas, 2011) using ArcGIS software. Class statistics were calculated for each initial state class and the final state image. Water levels were checked for imagery acquisition dates and times at Coastal Reference Monitoring System (CRMS; lacoast.gov/crms) water stations.

2.5. Field sediment sampling

Seven field sampling sites were selected based on their designation of land loss, land gain, or no change, as determined from the remote sensing analysis. Three sites (locations 1, 5, 7) had the additional advantage in that they were located ~500 m from monitoring stations run by the Coastwide Reference Monitoring Service (CRMS; lacoast.gov/crms), which collects data on water level, temperature, salinity, sediment rates, and vegetation pattern in a nearly continuous basis. Four to six short (~30 cm) push cores were collected at each of the seven field sites, totaling 36 short cores using hand-coring devices. Subtidal marshes were collected using a coring device with a 7 cm (ID) core barrel and subaerial cores were collected with a device with a 7.6 cm (ID) core barrel. Marsh position and elevation was determined using a real time kinematic (RTK) GPS; in cases were there marsh was flooded, water depths was measured with a meter stick. Cores were returned to the laboratory within 48 h of collect and kept in a cold room at ~4 °C until they were sampled.

Cores were cut lengthwise, with different analyses conducted on each half of the core. One half was subsampled at 2 cm intervals for the top 4 cm and then at 4 cm intervals down to a depth of 30 cm. In

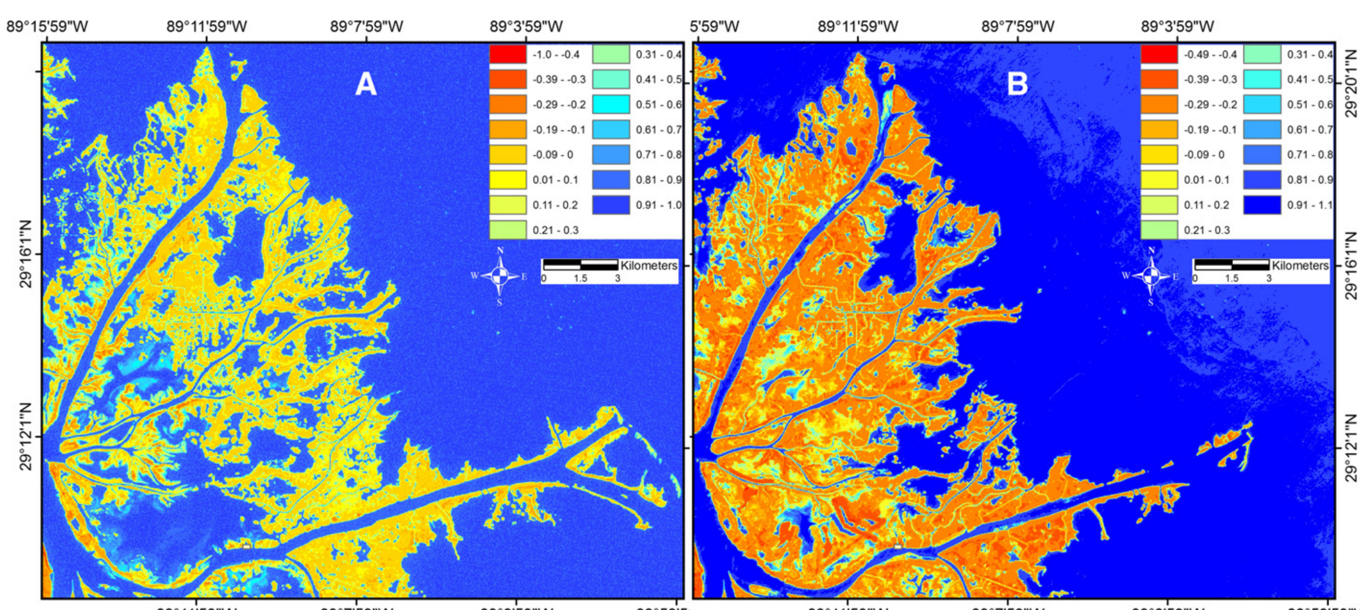

Fig. 2. Natural Difference Water Index (NDWI): A) 2000 Landsat ETM NDWI of Bands 1 (blue) and 5. B) 2015 Landsat OLI NDWI of Bands 2 (blue) and 6.

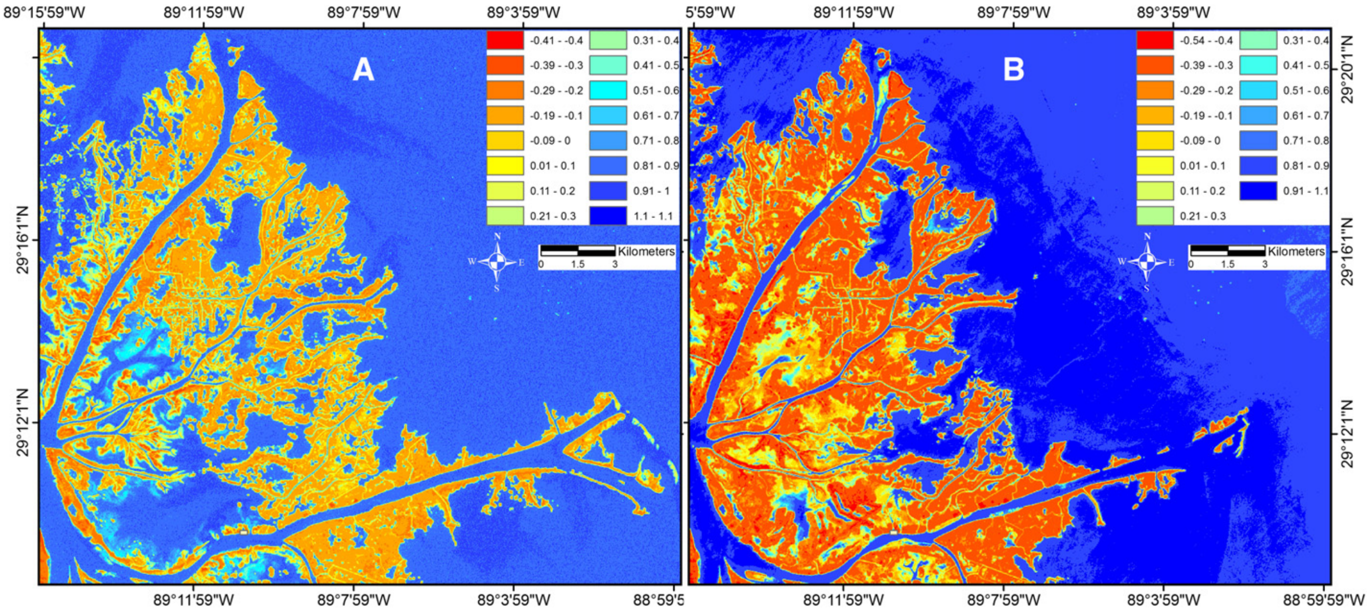

Fig. 3. Natural Difference Water Index (NDWI): A) 2000 Landsat ETM NDWI of Bands 2 (green) and 5. B) 2015 Landsat OLI NDWI of Bands 3 (green) and 6.

each interval water content was determined by drying samples to a constant weight at 60 °C; organic content was determined by combusting samples at 450 °C for 6 h, and bulk density was calculated using the water content and the fraction lost on ignition (LOI) using methods in Kolker et al. (2012). Aliquots of wet samples (~1 g) were removed from wet samples to be run for particle size analysis. Sediments were treated with 2 ml of H_20_2 for 8 h at room temperature to remove organics and 15 ml of $Na(PO_3)_6$, for 12 h at room temperature deflocculates fine particles, after which they were run on a Beckman-Coulter LS 13320 Laser Diffraction Particle Size Analyzer.

The second lengthwise half of the core was used to sample porewater salinity and to calculate sediment shear strength. Torque measurements using a Seiken shear vane pushed into the core half at 4 cm intervals and converted into shear strength using Eq. (10) (seikensha.com).

$$\tau = \frac{M_{max}}{\pi\left(\frac{\left(D^2H\right)}{2} + \frac{\left(D^3\right)}{6}\right)} \tag{10}$$

Where (τ) the shear strength (kN m^{-2}), Mmax is the maximum revolving moment (kN m^{-2}), D is the vane width (m), and H is the vane height (m). Porewater salinity was measured from the cores as a proxy for the long-term salinity of the marsh (Lara and Cohen, 2006). A sample was collected in the core half by extracting ~20 g of the sediment and spinning it at 2500 rpm in a centrifuge for ~5 min. Supernatant was removed via pipette and pore-water salinities were measured using a hand-held refractometer.

A Geographic Information Systems (GIS) spatial analyst inverse distance weighting (IDW) interpolation techniques was used to create surface maps of the geotechnical parameters including water content, LOI, salinity, bulk density, and shear strength. IDW is a deterministic interpolation methods based on the extent of similarity of cells using the linear-weighted combination set of sample points. The weight assigned is a function of the distance of an input point from the output cell location. The greater the distance, the less influence the cell has on the output value (ESRI.com).

3. Results

3.1. NDWI for water delineation

The newly developed Natural Difference Water Index (NDWI) was calculated for the Landsat 2000 ETM image and the 2015 OLI image using the natural difference between the highest and lowest reflectance bands (blue and SWIR) (Eq. (9); Fig. 2; Table 2). For comparison, this research also calculated the NDWI of (Eq. (3)) using bands (green and SWI; Fig. 3). The results indicated that the newly developed NDWI of (Eq. (9) was able to determine the water/land boundaries, and separate mixed water pixels better than the NDWI of Eq. (3). The NDWI values are a ratio that ranges from −1 to 1, with negative values (<0) indicating land that includes soil and vegetation, and positive values (>0) indicating water. In general, if the NDWI ranges from −1.0 to −0.2 the pixel is 100% land; if the NDWI ranges from −0.2 to 0.0 the pixel is a majority land and a minority water; if the NDWI is 0.0 to 0.49 the pixel is a majority water and a minority land; and if the pixel is 0.5 to 1.0 it is 100% water. While it is possible that sediment in river water could result in some water-dominated pixels being classified as land, we note the surface reflectance images of the area show reflectance in the blue band, and that the maximum difference between land and water occurs in the blue band, suggesting that this concern has not been manifested in this case (See supplemental data 2A and 2B). Pixels of water fractions 66%, 60%, and 55% have negative NDWI values (−0.01, −0.06, and −0.09), respectively (Figs 4 A&B). Pixels needed to include >90% water to be identified as, "water" because of the lower water reflectance of the green band than the blue band (Table 3). The results were evaluated using SPOT-7 high spectral resolution (6-m pixel size). SPOT-7 image was taken only one day before the Landsat OLI image. For overlay analysis, zoomin views of Landsat OLI NDWI (pixel size is 30-m) and SPOT-7 (pixel size is 6-m) were created where one OLI NDWI pixel include 18 SPOT-7 pixels which is equal to 1.6-m spatial resolution. The high spatial resolution zoomin SPOT-7 images show clearly the land/water transition at 1.6-m resolution and water fractions were calculated manually for the mixed water pixels. The overlay visualization analysis confirmed the Landsat NDWI thresholds (Fig. 4 C&D).

The Landsat 2000 ETM$^+$ and 2015 OLI NDWIs were classified into three classes (water, non-water (land), and mixed-water) based on the fractional water component (Fig. 5). The results of classified Landsat

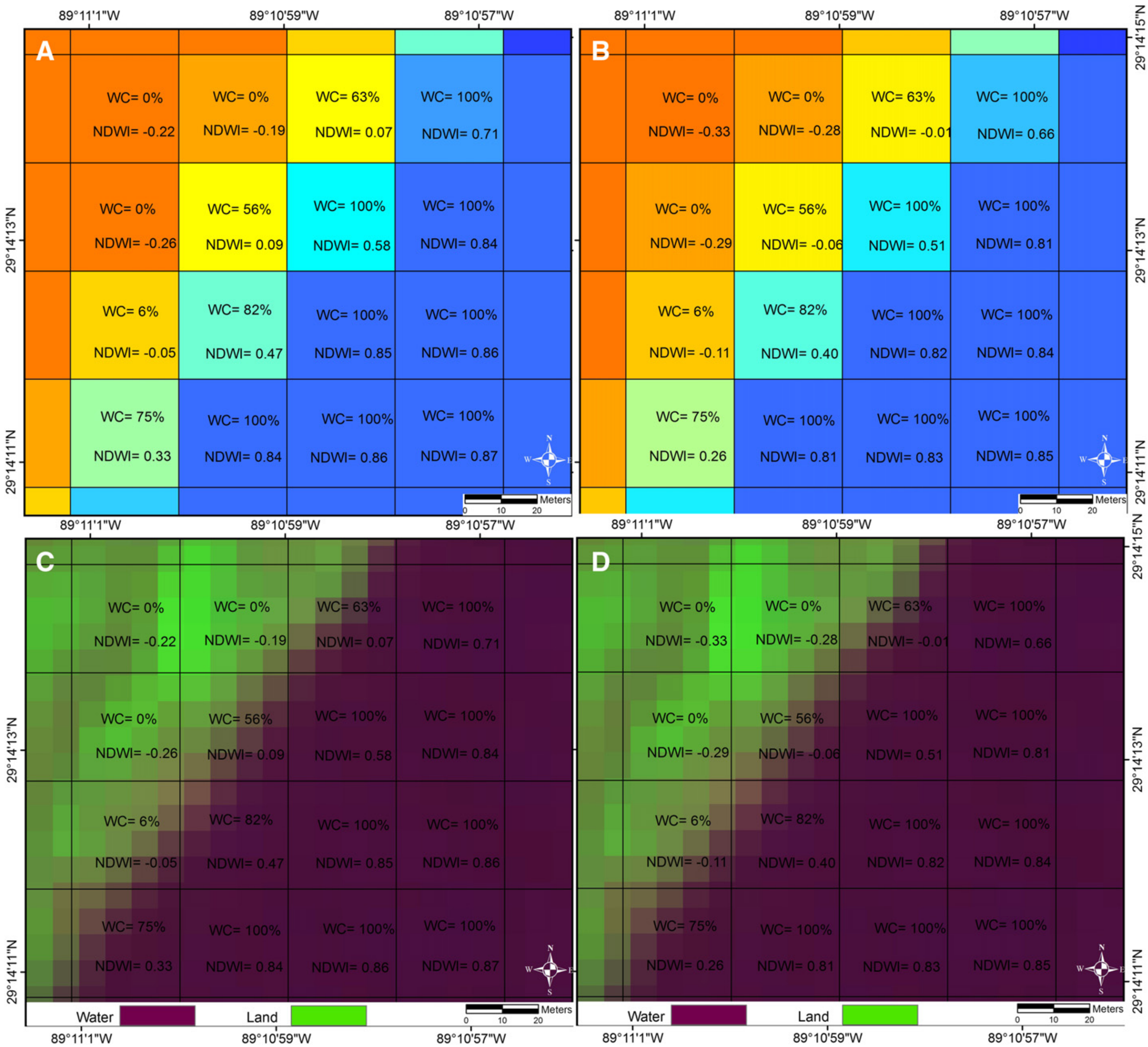

Fig. 4. Zoomed in view of Landsat OLI NDWI values and water area (WC) percentage in the pixel: A) 2015 Landsat OLI NDWI of Bands 2 (blue) and 6. B) 2015 Landsat OLI NDWI of Bands 3 (green) and 6. C) SPOT-7 zoomin view of the same area of Fig. A. D) SPOT-7 zoomin view of the same area of Fig. B.

2000 ETM$^+$ NDWI show that the water class covers about 73.3%, the land (non-water) 19.02%, and mixed-water 7.5% while the classified 2015 OLI NDWI has 68.3 water, 23.1 land, and 8.4 mixed-water (Table 4). Classification accuracy assessments using the confusion matrix were performed on the 2000 and 2015 Landsat NDWI classified maps to quantify the reliability of the data sets (Supplementary Tables 2&3). The overall accuracies of all classified maps were above 99% confidence level, and Kappa statistics are well above 0.9. The classification accuracy reflects how well the water, non-water and mixed-water classes were identified from the newly developed NDWI.

3.2. Change detection of land/water changes

The Landsat 2000 ETM$^+$ classified NDWI was subtracted from the 2015 OLI classified NDWI using GIS spatial analysis to quantify land loss changes. Each pixel in the classified maps was compared on a pixel-by-pixel basis. A resultant spatial trend data set is created identifying the changes among the classified land and water data sets. A change pixel was classified as: (1) land changed to water (loss), (2) mixed-water changed to water (loss), (3) land to land or water to water (no change), (4) water changed to land (gain), or (5) mixed-water changed to land (gain) (Table 5; Fig. 6).

The study area is about 589.5 km^2, and encompasses all of the CGSD and surrounding environments. This remote sensing analysis indicates that in the fifteen year between 2000 and 2015, the CGSD experienced about 84-km^2 of land gain that represents approximately 14.2% of the total area. About 29.1 km^2 (4.9%) of water areas changed to land, and 54.9 km^2 (9.3%) of mixed water/land areas changed into permanent land. Land gains were predominantly located in three settings: (1) crevasse splays cut in subchannels in the central delta (e.g., Octave Pass and Brant's Pass), (2) infilled canals along the west flank of Main Pass, and (3) dredge spoil zones in southwestern delta. There is about 38.1 km^2 land loss which represents approximately 6.4% of the study area. There are about 21.0 km^2 (3.5%) of land, and 17.1 km^2 (2.9%) of

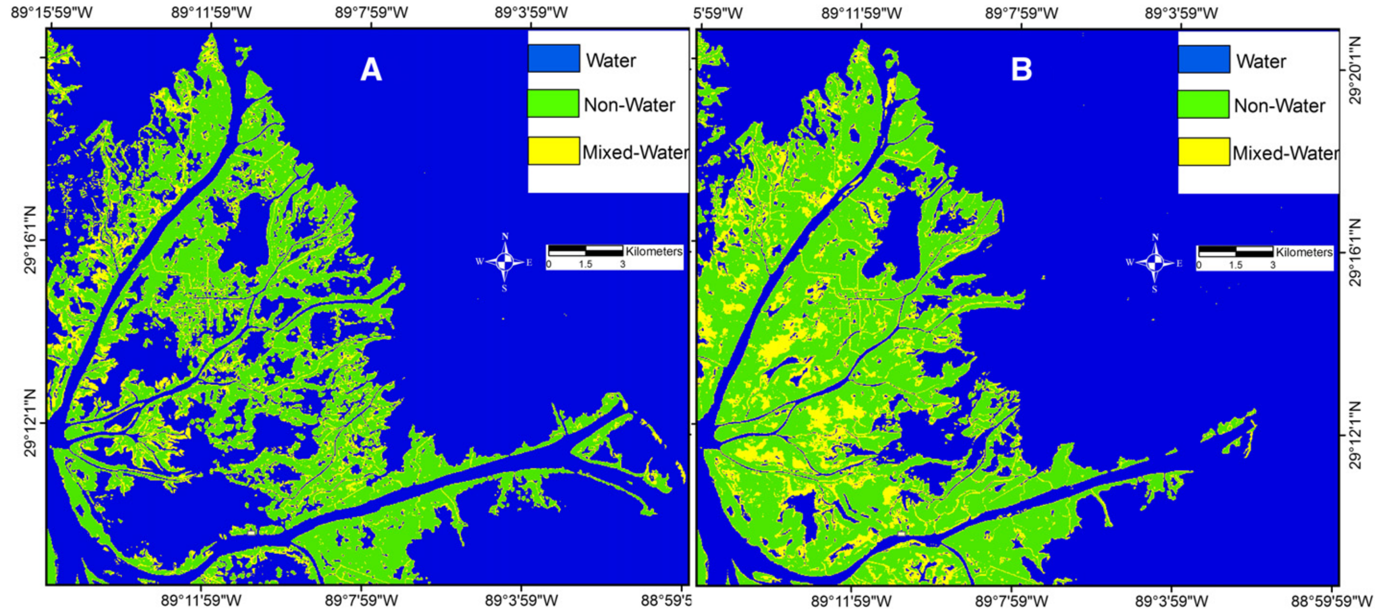

Fig. 5. Landsat NDWI classified map: A) 2000 Landsat ETM$^+$. B) 2015 Landsat OLI.

wetlands changed into permanent water. Land loss is typically found in (1) ocean-fringing marshes, or (2) at the border of large ponds along the eastern edge of the CGSD.

3.3. Geotechnical results

The properties of all cores are summarized here, with a particular focus on the top 16 cm, which roughly corresponds to the active rooting zone and the area of maximum impacts during Hurricane Katrina (Howes et al., 2010; Turner et al., 2007). The data are available in full in the supplementary material. Water content ranged from 18.3 to 87.9%, with an average value of 49.0 ± 14.0 for the top 16 cm of the 30 primary cores. Water content decreased with depth in 10 cores and increased with depth in 5 cores (Supplementary Table 4 and Fig. 4). Loss on ignition (LOI) values ranged from 0.48 to 79.0%, and averaged 8.8 ± 13.3% for all the top 16 cm of the 30 primary cores. Shear strength ranged from 0.21 to 35.4 kN m^{-2} and averaged 8.0 ± 5.1 kN m^{-2} for the top 16 cm of the 30 cores. The cores with the lowest shear strength were 7B, 5D, and 6C, and the cores with the highest shear strength 2C, 2D, 3C, and 3E. Overall, bulk density ranged from 0.12 to 1.63 g cm^{-3} and averaged 0.79 g cm^{-3}. Across all cores, porewater salinity ranged from 0 to 15.88 ppt and averaged ~4 ppt. The sediments from CGSD were composed of sandy silts; the average median grain size for all core intervals was 32.0 ± 17.3 mm, and whiles the mean grain size for the top 16 cm of all cores was 30.8 ± 15.4. The average d10 was 1.6 ± 1.0 mm for all cores and 1.7 ± 1.1 for the top 16 cm, while the average d90 was 87.3 ± 71.3 mm for all cores and 75.1 ± 42.1 mm for the top 16 cm. Overall, water content and organic content are positively and strongly correlated (Supplementary Fig. 5). Bulk density and shear strength are strongly correlated, as are water content and shear strength. Though the relationship between LOI and shear strength suggests a correlation, it is not significant at the $p < 0.05$ level. There are no significant relationships between grain size and either shear strength, water content, LOI, bulk density.

The distance from the Mississippi River was a strong predictor of geotechnical properties (Supplementary Fig. 6). Water content and LOI were significantly and positively related to the distance from the Mississippi River, whereas shear strength and bulk density were negatively related to the distance from the Mississippi River. Areas with land loss generally correlate to high values of average water content, LOI, and salinity, where areas of land gain generally correlate to lower values (Fig. 7 a, b and c). Areas with high shear strength and bulk density correlate to areas of land gain, where areas of land loss correlate to low shear strength and bulk density values (Fig. 7 d and e).

4. Discussion

4.1. Land area change in Louisiana

Coastal Louisiana has experienced large-scale changes in land area over the past century (Reed, 2002, LACPRA 2017, Couvillion et al., 2011, Roberts, 1997). The system is dominated by land loss, which has been linked to numerous drivers that include high rates of relative sea-level rise, reduced rates of sediment deposition, the construction of canals, hydrological changes, eutrophication, invasive species, and wave driven erosion (Reed, 2002; Tornqvist et al., 2007; Kolker et al., 2011; Darby and Turner, 2008; Day et al., 2007). Land gain is largely confined to small areas near the mouth of the Mississippi and Atchafalaya Rivers, including the CGSD (Wells and Coleman, 1987; Day et al., 2007; Kolker et al., 2011; Wellner et al., 2005).

Table 2
Reflectance % of water and land transects on Landsat ETM$^+$ and Landsat OLI bands measured at location of the field sites.

Sensor	Landsat-7 ETM$^+$						Landsat-8 OLI					
Band	B1	B2	B3	B4	B5	B7	B2	B3	B4	B5	B6	B7
	Blue	Green	Red	NIR	SWIR	SWIR	Blue	Green	Red	NIR	SWIR	SWIR
Water ref%	0.13	0.10	0.080	0.03	0.040	0.002	0.10	0.083	0.068	0.02	0.004	0.003
Land ref%	0.12	0.09	0.079	0.13	0.137	0.057	0.95	0.074	0.064	0.16	0.150	0.084

Table 3
Hypothetical example of mixed water/land pixels.

Category	Pure water	Water fraction	Land fraction	Pure land
Pixel		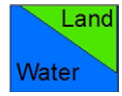	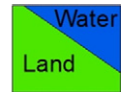	
Water area in the pixel	100% water	Water > land	Land > water	100% land
NDWI value	1.0–0.5	0.49–0	0 to −0.2	−0.2 to −1.0

Land change processes in the CGSD are particularly interesting to study because it is an analogue for the kind of large-scale river diversion that is envisioned by Louisiana's Master Plan for a Sustainable Cost (LACPRA 2017). The average discharge into Cubit's Gap is 1650 m^3 s^{-1} (58,000 ft^3 s^{-1}), whereas many of the diversions envisioned by Louisiana's Master Plan have maximum capacities of 1420–2100 m^3 s^{-1} (50,000–75,000 ft^3 s^{-1}; LAPCRA 2012, LACPRA, 2017, Esposito et al., 2013, Allison et al., 2012) The CGSD is also experiencing both land loss and land gain, which allows one to address the controversies around the influence of river inputs and hurricanes on land development and erosion in the Mississippi River Delta (Howes et al., 2010; Turner et al., 2006; Tornqvist et al., 2007). Specifically, this study tested the hypothesis that areas of land gain in the CGSD received high inputs of mineral-rich river water, whereas areas of land loss were located in areas with reduced mineral inputs and high exposure to storms. This hypothesis was tested using multiple analyses of the data.

4.2. Relationships between land change and sediment properties

In the first analysis, this team of authors examined the relationship between geotechnical properties and the distance to the Mississippi River. This analysis found that bulk density and shear strength decrease in a statistically significant manner from the mouth of the river, and that water content and LOI increase in a statistically significant fraction from the mouth of the river. These findings indicate that marshes near the mouth of the river are dominated by high mineral inputs that result in dense soils that are relatively resistive to erosion whereas marshes that are distal to the river are dominated by organic soils that are relatively prone to erosion. Though one might expect to find coarser sediment closer to the river, this analysis found no statistically significant relationship between distance to the river and particle size- perhaps because the sediment loads in the Mississippi River are dominated by fine particles (<63 um) most of the year.

To further examine the controls on land loss and land gain, this team of authors specifically compared the geotechnical parameters for samples collected in areas of land gain, land loss and areas of no change (Table 6, Supplemental Fig. 6). Using a 1-tailed *t*-test that assumed unequal variances, this analysis found that areas of land loss had significantly ($p < 0.05$) greater water content, higher loss on ignition and lower bulk density. Shear strength appeared to be lower in the areas of marsh loss, though the trend was not statistically significant ($0.10 < p < 0.15$). A similar pattern emerges in box and whisker plots of the same data.

To further understand the spatial configuration of geotechnical properties and their association with areas of land loss and land gain, geospatial maps of each were created (Fig. 7). These maps present the average value for the top 16 cm of each core, and the ArcGIS- spatial analyst inverse distance weighting (IDW) algorithm was used to interpolate raster surfaces from the geotechnical parameters of the core points. This method assumes that the geotechnical parameter being mapped decreases in influence with distance from its core location. These maps show that marshes near the river tend to have lower water contents, low LOI values, low salinities, higher bulk densities and high shear strength values. Furthermore areas of land gain are largely concentrated near the Mississippi River whereas areas of land loss generally occur near the distal region of the delta.

The most parsimonious explanation for these data is that marshes near the Mississippi River are dominated by alluvial sedimentary processes, whereas marshes near the distal edge of the delta are generally organic accumulation, and prone to storm and wave induced erosion (Fig. 8). Riverine processes deliver mineral sediments to marshes, and while channels can carry sand up to 6 km from the mouth of the river (Esposito et al., 2013), much of the material is deposited close to the river. As such, these wetlands are dominantly mineral rich, with high bulk densities, high shear strengths that are geomorphically stable, or prograding. On the other hand, the distal marshes have fewer mineral inputs, which yields wet, organic rich settings. The lack of mineral inputs means that there is relatively little material for marsh development, and their seaward exposure means that land loss is likely to occur during storms and wave events. While the results of this study cannot explain all of the causes of wetland change in the Mississippi River Delta (e.g. loss caused by canal construction, high rates relative sea level rise, or oil spills, or gain caused by vegetative colonization of emergent habitat), they provide insights into how one critical habitat, river-dominated coastal wetlands, function, grow and erode.

4.3. Implication of findings to coastal restoration in the Mississippi River Delta

These findings have important implications for the restoration of coastal wetlands in Louisiana, which has lost nearly 4900 km^2 of wetlands over the past century (Couvillion et al., 2011). This land loss makes the Mississippi River Delta one of the most rapidly changing environments on earth (Giosan et al., 2014; Syvitski and Saito, 2007). There were numerous causes of this land loss, including high rates of relative sea level rise, reduced rates of sediment deposition, hurricane

Table 4
Summary of Landsat 2000 ETM^+ and 2015 OLI NDWIs classifications.

Class	Landsat 2000 ETM^+ NDWI Classes		Landsat 2015 OLI NDWI Classes	
	Area (km)	Percent (%)	Area (km)	Percent (%)
Non-water	112.1283	19.021148	136.5822	23.169443
Mixed-water	44.7975	7.599329	50.0418	8.488959
Water	432.567	73.379522	402.8688	68.341598
Total	589.4928	100	589.4928	100

Table 5
Land loss and land gain trends from 2000 to 2015.

Land Loss/Gain Change		
Class	Area (km)	Percent (%)
Land changed to water (loss)	21.0	3.6
Mixed-water changed to water (loss)	17.1	2.9
No change	467.2	79.2
Mixed-water changed to land (gain)	55.0	9.3
Water changed to land (gain)	29.2	5.0
Total	589.5	100

Table 6
Average geotechnical values for land gain, no change, and land loss cores.

	% water content	% LOI	Bulk density (g/cm^3)	Shear strength (kN m^{-2})	Porewater salinity (ppt)	Mean grain size (um)
Land gain	38.1 ± 4.20	3.91 ± 0.61	1.00 ± 0.11	10.9 ± 4.12	0.22 ± 0.15	30.1 ± 5.90
No change	47.9 ± 2.91	10.3 ± 3.81	0.75 ± 0.05	8.25 ± 1.19	2.92 ± 0.87	65.9 ± 19.3
Land loss	54.8 ± 3.68	9.03 ± 1.88	0.64 ± 0.07	5.67 ± 0.79	6.53 ± 1.99	31.0 ± 3.25

and storm-driven erosion, salt water intrusion and eutrophication (Reed, 2002; Day et al., 2007; Kolker et al., 2011; Tornqvist et al., 2007; Turner et al., 2006; Turner et al., 2007). Restoration of Louisiana's wetlands depends, in part, on plans to partially divert the Mississippi River, which would bring new sediments into previously degrading wetlands, thereby restarting natural deltaic land building processes (LACPRA et al., 2012). River floods in crevasses in the Mississippi River Delta can deliver regularly deliver 1–5 cm of sediment- enough to offset regional rates of relative sea level rise (Kolker et al., 2012; Esposito et al., 2013; Kolker et al., 2014; Rosenheim et al., 2013; Smith et al., 2015), with extreme floods capable of delivering nearly 60 cm of sediment (Day et al., 2016a).

However, this view is not without controversy. Several authors noted that freshwater marshes in the flow path of the Caernarvon Freshwater Diversion experienced higher rates of wetlands loss than nearby salt marshes outside of the diversion's flow path (Kearney et al., 2011; Howes et al., 2010; Barras, 2006). One school of thought holds that these losses were driven by the freshwater diversion, and that fresh marshes that receive nutrient-rich river water are less biophysically stable than salt marshes (Kearney et al., 2011; Darby and Turner, 2008). This view holds that other river diversions would likely lead to marsh loss rather than the intended marsh gain (Turner et al., 2006; Turner et al., 2007). An alternate view holds that the Caernarvon-influenced marshes experienced marsh loss during Hurricane Katrina because they were mineral poor marshes, and that this lack of mineral matter contributed to their stability. This view holds that marshes under the influence of larger diversions that are capable of transporting larger quantities of sediment should be more resilient to hurricane impacts (Day et al., 2016b). Indeed, many of the planned diversions are orders of magnitude larger than the Caernarvon Diversion (LACPRA 2017). The results of this study supports into the latter view, that introducing mineral inputs via to wetlands via large river diversions makes them more resilient erosion, and that marshes with lower mineral contents are less resilient to storm and wave driven erosion. Furthermore, results from this study suggest that the salinity of the wetlands is not, in itself, a control on resilience to erosion (Turner et al., 2007); instead the controlling parameters appears to be whether freshwater inputs are mineral-rich or not.

These findings have applications to river deltas globally, which are major loci of commerce, fisheries, industry and are home to nearly 500 million people (Giosan et al., 2014). Many river deltas are losing land, and efforts to restore these systems are often consistent with those in employed in the Mississippi River Delta (Giosan et al., 2014). As such, strategies to study land area change in systems worldwide are likely to couple in-situ geotechnical work with remote sensing algorithms, including, but not limited to, those presented herein.

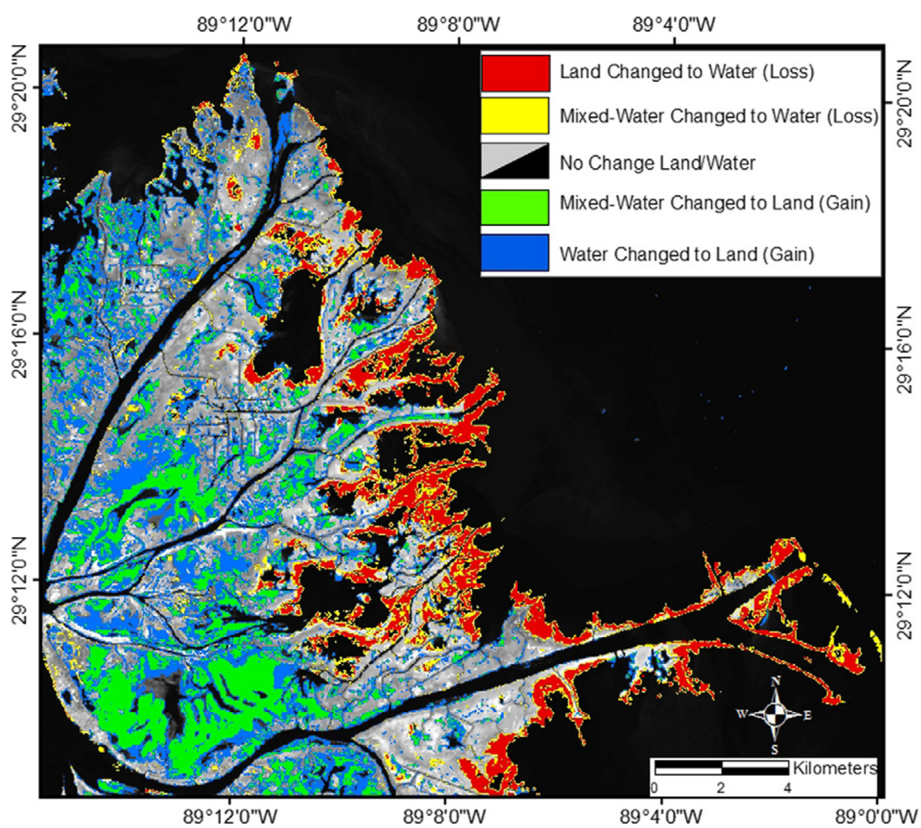

Fig. 6. Land loss and gain change map of the Cubit's Gap Subdelta (CGSD).

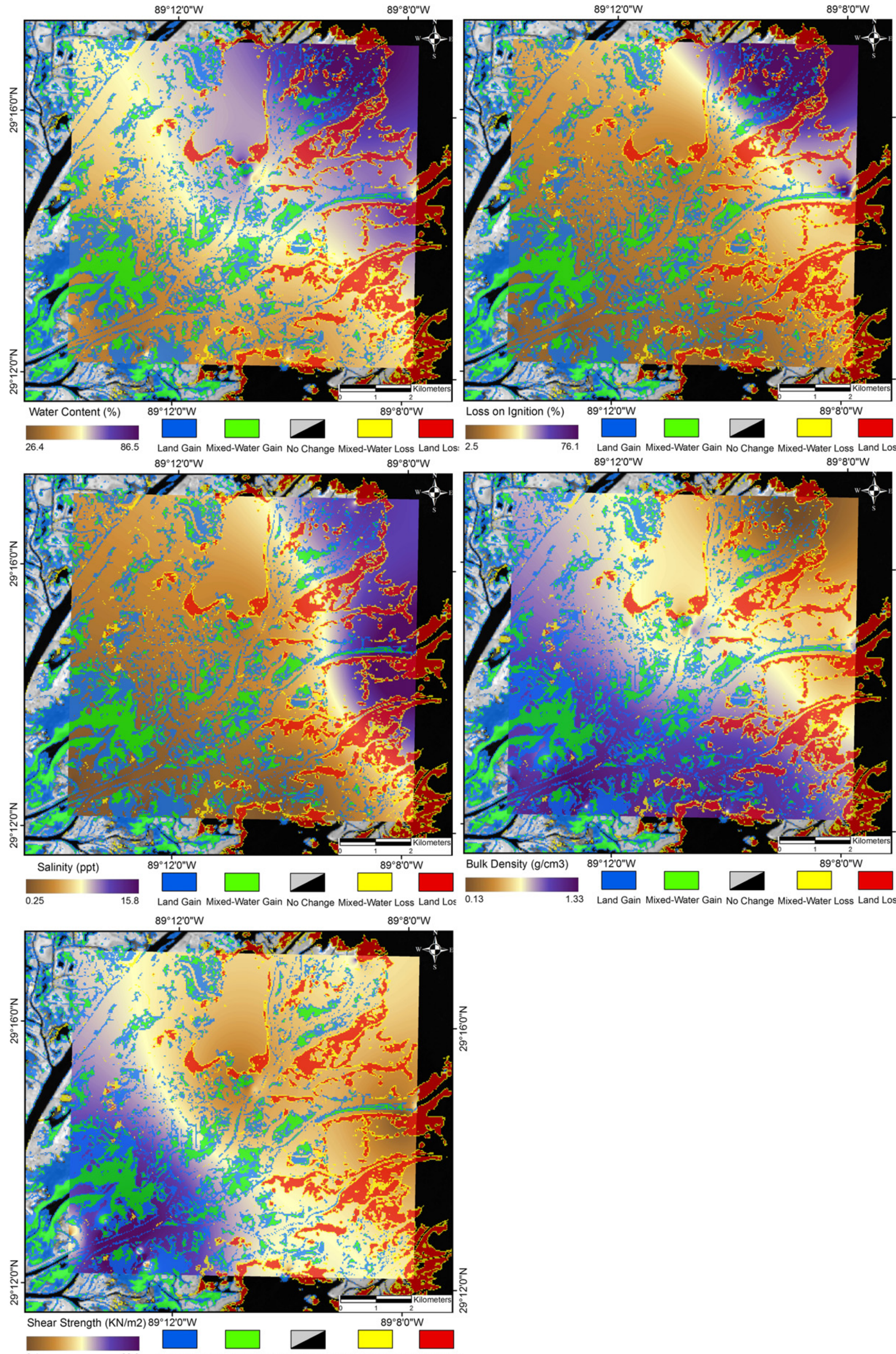

Fig. 7. Geotechnical parameters overlying the land loss and gain change map of the CGSD: a) water content; b) loss of ignition; c) salinity; d) bulk density; and e) shear strength.

5. Conclusion

This study led to the following specific advances:

1) A new Normalized Difference Water Index (NDWI), based on blue and SWIR bands for pure water, land (vegetation and soil), and mixtures of these components was created. Results indicated that the newly developed NDWI was able to determine water/land boundaries, better than the previously published NDWI. Given that coastal change in a global phenomena (e.g.Nicholls and Cazenave, 2010), this newly developed NDWI may improve the scientific communities ability to map land/water boundaries globally.
2) Using this new NDWI as a guide to, this research examined geotechnical properties of sediments in the Mississippi River Delta and found that areas that were developing land or were resistant to erosion were dominated by mineral-rich soils whereas sediments that were erosion prone were dominated by organic deposits. Mineral-rich sediments tended to be proximal to the Mississippi River whereas organic-rich sediments tended to be distal to it.
3) Results from this study suggest that hydrological restorations of the Mississippi River Delta will be most effective if they include both Mississippi River water and high sediment loads.

Acknowledgements

This work was supported by the Louisiana Universities Marine Consortium and the Mississippi River Delta Coalition. Many thanks to M.A. Allison and S. Nelson of Tulane University who reviewed an earlier draft of this manuscript.

Appendix A. Supplementary data

Supplementary data to this article can be found online at http://dx.doi.org/10.1016/j.rse.2017.06.030.

References

Allison, M.A., Meselhe, E.A., 2010. The use of large water and sediment diversions in the lower Mississippi River (Louisiana) for coastal restoration. J. Hydrol. 387, 346–360.

Allison, M.A., Demas, C.R., Ebersole, B.A., Kleiss, B.A., Little, C.D., Meselhe, E.A., Powerll, N.J., Pratt, T.C., Vosberg, B.M., 2012. A water and sediment budget for the lower Mississippi-Atchafalaya River in flood years 2008–2010: implications for sediment discharge and coastal restoration in Louisiana. J. Hydrol. 432–433, 84–97.

Atkinson, B., Mahony, D., 2004. S — Plus ROC Functions. Mayo Foundation for Medical Education and Research, Rochester, MN.

Barras, J., 2006. Land area change in coastal Louisiana after the 2005 hurricanes: a series of three maps. US Geological Survey Open File Report 06–1274.

Barras, J., Beville, S., Britsch, D., Hartley, S., Hawes, S., Johnston, J., Kemp, P., Kinler, Q., Martucci, A., Porthouse, J., Reed, D., Roy, K., Sapkota, D., Suhayda, J., 2003. Historical and projected coastal Louisiana land changes-1978–2050. Appendix B of Louisiana Coastal Area (LCA), Louisiana Ecosystem Restoration Study: U.S. Geological Survey Open-File Report 2003-334 (39 p.).

Boyer, M.E., Turner, R.E., 1995. Data on crevasse splays in the Delta National Wildlife Refuge, Mississippi River Delta. Final report to the United States Environmental Protection Agency, Dallas, Texas.

Britsch, L.D., Dunbar, J.B., 1993. Land-loss rates-Louisiana coastal plain. J. Coast. Res. 9, 324–338.

Congalton, R.G., 1991. A review of assessing the accuracy of classification of remotely sensed data. Remote Sens. Environ. 1991 (37), 35–46.

Coppin, P., Jonckheere, I., Nackaerts, K., Muys, B., 2004. Digital change detection methods in ecosystem monitoring: a review. Int. J. Remote Sens. 25 (9), 1565–1596.

Couvillion, B.R., Barras, J.A., Steyer, G.D., Sleavin, W., Fischer, M., Beck, H., Trahan, N., Griffin, B., Heckman, D., 2011. Land area change in coastal Louisiana from 1932 to 2010. U.S. Geological Survey Scientific Investigations Map 3164, Scale 1:265,000 (12 p).

Darby, F.A., Turner, R.E., 2008. Below- and aboveground biomass of *Spartina alterniflora*: response of nutrient addition in a Louisiana salt marsh. Estuar. Coasts 31, 326–334.

Day, J.W., Boesch, D.F., Clairain, E.J., Kemp, G.P., Laska, S.B., Mitsch, W.J., Orth, K., Mashriqui, H., Reed, D.J., Shabman, L., Simenstad, C.A., Streever, B.J., Twilley, R.R., Watson, C.C., Wells, J.T., Whigham, D.F., 2007. Restoration of the Mississippi Delta: lesson from Hurricanes Katrina and Rita. Science 315, 1679–1684.

Day, J.W., Cable, H.E., Lane, R.R., Kemp, G.P., 2016a. Sediment deposition at the Caernarvon Crevasse during the great Mississippi Flood of 1927: implications for coastal restoration. WaterSA 8:38. http://dx.doi.org/10.3390/w8020038.

Day, J.W., Lane, R.R., D'Elia, C.F., Wiegman, A.R.H., Rutherford, J.S., Shaffer, G.P., Brantley, C.G., Kemp, G.P., 2016b. Large infrequently operated river diversions for Mississippi delta restoration. Estuar. Coast. Shelf Sci. http://dx.doi.org/10.1016/j.ecss.2016.05.001.

Esposito, C.R., Georgiou, I.Y., Kolker, A.S., 2013. Hydrodynamic and geomorphic controls on mouth bar evolution. Geophys. Res. Lett. 40, 1540–1545.

Foody, G.M., 2002. Status of land cover classification accuracy assessment. Remote Sens. Environ. 80, 185–201.

Giosan, L., Syvitski, J., Constantinescu, S., Day, J., 2014. Climate change: protect the world's deltas. Nature 516 (7529), 31–33.

Howes, N.C., FitzGerald, D.M., Hughes, Z.J., Georgiou, I.Y., Kulp, M.A., Miner, M.D., Smith, J.M., Barras, J.A., 2010. Hurricane-induced failure of low salinity wetlands. Proceedings of the National Academy of Sciences U.S.A. 107, pp. 14014–14019.

Jensen, J.R., 1996. Introductory Digital Image Processing: a Remote Sensing Perspective. 2nd edition. Prentice Hall, Upper Saddle River, New Jersey.

Ji, L., Zhang, L., Wylie, B., 2009. Analysis of dynamic threshold for the Normalized Difference Water Index. Photogramm. Eng. Remote. Sens. 75, 1307–1317.

Kearney, M.S., Riter, J.C.A., Turner, R.E., 2011. Freshwater river diversions for marsh restoration in Louisiana: twenty-six years of changing vegetative cover and marsh area. Geophys. Res. Lett. 38, L16405.

Kim, W., Mohrig, D., Twilley, R., Paola, C., Parker, G., 2009. Is it feasible to build new land in the Mississippi River Delta? Eos. Trans. AGU 90, 373–374.

Klemas, V., 2011. Remote sensing of wetlands: case studies comparing practical techniques. J. Coast. Res. 27 (3), 418–427.

Kolker, A.S., Allison, M.A., Hameed, S., 2011. An evaluation of subsidence rates and sea-level variability in the northern Gulf of Mexico. Geophys. Res. Lett. 38, L21404. http://dx.doi.org/10.1029/2011GL049458.

Kolker, A.S., Miner, M.D., Weather, H.D., 2012. Depositional dynamics in a river diversion receiving basin: the case of the West Bay Mississippi River Diversion. Estuar. Coast. Shelf Sci. 106, 1–12.

Kolker, A.S., Li, C., Walker, N.D., Pilley, C., Ameen, A., Boxer, G., Ramatchandirane, C.G., Ullah, M., Williams, K.A., 2014. The impacts of the great Mississippi/Atchafalaya River flood on the oceanography of the Atchafalaya Shelf. Cont. Shelf Res. 86, 17–33.

LACPRA, 2017. Louisiana's Comprehensive Master Plan for a Sustainable Coast. Louisiana Coastal Restoration and Protection Authority, Baton Rouge.

Lara, R.J., Cohen, M.C.L., 2006. Sediment porewater salinity, inundation frequency and mangrove vegetation height in Braganca, North Brazil: an ecohydrology-based empirical model. Wetl. Ecol. Manag. 14, 349–358.

Mather, P., 2004. Computer Processing of Remotely-Sensed Images, 2004. John Wiley & Sons, Ltd.

McFeeters, S.K., 1996. The use of Normalized Difference Water Index (NDWI) in the delineation of open water features. Int. J. Remote Sens. 17 (7), 1425–1432.

Memarsadeghi, N., Netanyahu, N.S., LeMoigne, J., 2006. A fast implementation of the ISODATA clustering algorithm. Int. J. Comput. Geom. Appl. 17 (1), 71–103, 2007.

Nicholls, R.J., Cazenave, A., 2010. Sea-level rise and its impact on coastal zones. Science 328 (5985), 1517–1520.

Ouma, Y.O., Tateishi, R., 2006. A water index for rapid mapping of shoreline changes of five East African Rift Valley lakes: an empirical analysis using Landsat TM and ETM data. Int. J. Remote Sens. 27 (15), 3153–3181.

Palaneasu-Lovejoy, M., Kranenburg, C., Barras, J.A., Brock, J.C., Brock, J.C., Barras, J.A., Williams, S.J., 2013. Land loss due to recent hurricanes in coastal Louisiana, U.S.A. Understanding and Predicting Change in the Coastal Ecosystems of the Northern Gulf of Mexico, Journal of Coastal Research, Special Issue No. 63, pp. 97–109.

Palaseanu-Lovejoy, M., Kranenburg, C., Brock, J.S., Barras, J.A., 2011. Recent wetland land loss due to hurricanes: improved estimates based upon multiple source images. Proceedings of Coastal Sediments 2011 (Miami, Florida). Vol. 3, pp. 2253–2270.

Plourde, L., Congalton, R.G., 2003. Sampling method and sample placement: how do they affect the accuracy of remotely sensed maps? Photogramm. Eng. Remote. Sens. 69, 289–297.

Reed, D.J., 2002. Sea-level rise and coastal marsh sustainability: geological and ecological factors in the Mississippi delta plain. Geomorphology 48, 233–243.

Roberts, H.H., 1997. Dynamic changes of the Holocene Mississippi River delta plain: the delta cycle. J. Coast. Res. 13, 605–627.

Rogers, A.S., Kearney, M.S., 2004. Reducing signature variability in unmixing coastal marsh Thematic Mapper scenes using spectral indices. Int. J. Remote Sens. 25 (12), 2317–2335.

Rosenheim, B.E., Roe, K.M., Roberts, B.J., Kolker, A.S., Allison, M.A., Johannesson, K.H., 2013. River discharge influences on particulate organic carbon age structure in the Mississippi/Atchafalaya River system. Glob. Biogeochem. Cycles 27, 154–166.

Smith, H., Bentley, S.J., Snedden, G.A., White, C., 2015. What role do hurricanes paly in sediment delivery to subsiding river deltas. Sci Rep 5, 17582.

Syvitski, J.P.M., Saito, Y., 2007. Morphodynamics of deltas under the influence of humans. Glob. Planet. Chang. 57, 261–282.

Teal, J.M., Best, R., Caffrey, J., Hopkinson, C.S., McKee, K.L., Morris, J.T., Newman, S., Orem, B., 2012. Mississippi River freshwater diversions in Southern Louisiana: effects on wetland vegetation, soils, and elevation. In: Lewitus, A.J., Croom, M., Davison, T., Kidwell, D.M., Kleiss, B.A., Pahl, J.W., Swarzenski, C.M. (Eds.), Final Report to the State of Louisiana and the U.S. Army Corps of Engineers through the Louisiana Coastal Area Science & Technology Program; coordinated by the National Oceanic and Atmospheric Administration (49 pages).

Tornqvist, T.E., Paoloa, C., Parker, G., Liu, K., Mohrig, D., Holbrook, J.M., Twilley, R.R., 2007. Comment on, "Wetland sedimentation from Hurricanes Katrina and Rita,". Vol. 316 pp. 201–202.

Turner, R.E., 1997. Wetland los in the Northern Gulf of Mexico: multiple working hypotheses. Estuaries 20, 1–13.

Turner, R.E., Baustain, J.J., Swenson, E.M., Spicer, J.S., 2006. Wetland sedimentation from Hurricanes Katrina and Rita. Science 314, 449–452.
Turner, R.E., Swensen, E.M., Milan, C.S., Lee, J.M., 2007. Hurricane signals in salt marsh sediments: inorganic sources and soil volume. Limnol. Oceanogr. 53, 1231–1238.
Wellner, R., Beaubouef, R., Wagoner, V., Roberts, H., Tao, S., 2005. Jet-plume depositional bodies - the primary building blocks on Wax Lake Delta. Gulf Coast Association of Geological Societies Transactions 55, 867–909.
Wells, J.T., Coleman, J.M., 1987. Wetland loss and the subdelta life cycle. Estuar. Coast. Shelf Sci. 25, 111–125.
Xu, H., 2006. Modification of normalised difference water index (NDWI) to enhance open water features in remotely sensed imagery. Int. J. Remote Sens. 27 (14), 3025–3033.